Compatibilization of highly sustainable polylactide/almond shell flour composites by reactive extrusion with maleinized linseed oil

QUILES-CARRILLO, Luis J, MONTANES, Nestor, SAMMON, Chris <http://orcid.org/0000-0003-1714-1726>, BALART, Rafael and TORRES-GINER, Sergio

Published version

QUILES-CARRILLO, Luis J, MONTANES, Nestor, SAMMON, Chris, BALART, Rafael and TORRES-GINER, Sergio (2017). Compatibilization of highly sustainable polylactide/almond shell flour composites by reactive extrusion with maleinized linseed oil. Industrial Crops and Products, 111, 878-888.

Industrial Crops & Products, 111 (2018) 878–888

http://dx.doi.org/10.1016/j.indcrop.2017.10.062

Compatibilization of highly sustainable polylactide/almond shell flour composites by reactive extrusion with maleinized linseed oil

L. Quiles-Carrillo[1], N. Montanes[1], C. Sammon[2], R. Balart[1], S. Torres-Giner[3,4*]

[1] Technological Institute of Materials (ITM), Universitat Politècnica de València (UPV), Alcoy, Spain

[2] Materials and Engineering Research Institute, Sheffield Hallam University, Sheffield, UK.

[3] Novel Materials and Nanotechnology Group, Institute of Agrochemistry and Food Technology (IATA), Spanish National Research Council (CSIC), Paterna, Spain

[4] School of Technology and Experimental Sciences (ESTCE), Universitat Jaume I (UJI), Castellón, Spain

* Corresponding author: storresginer@iata.csic.es

Abstract. Highly sustainable composites were produced by melt compounding polylactide (PLA) with almond shell flour (ASF), a processed byproduct of the food industry, at a weight content of 30 wt.-%. However, due to the lack of miscibility between PLA and ASF, both being raw materials obtained from crops, resultant green composite presented poor ductility and low thermal stability. To overcome this limitation, maleinized linseed oil (MLO), a multi-functionalized plant-derived additive, was originally incorporated as a reactive compatibilizer during the extrusion process. Both chemical and physical characterizations showed that 1–5 parts per hundred resin (phr) of MLO successfully serve to function as a novel compatibilizer on the PLA/ASF composites, leading to highly sustainable materials with balanced mechanical, thermal, and thermomechanical properties. Achieved compatibilization was particularly related to a dual effect of plasticization in combination with grafting. The latter effect was ascribed to the formation of new carboxylic ester bonds through the reaction of the multiple maleic anhydride groups present in MLO with the hydroxyl terminal groups of both PLA chains and lignocellulose on the ASF surface. The fully bio-based and

biodegradable composites described herein give an efficient sustainable solution to upgrade agro-food wastes as well as contributing to reducing the cost of PLA-based materials.

Keywords: *PLA, Lignocellulosic fillers, Green composites, Multi-functionalized vegetable oils, Reactive extrusion, Waste valorization*

1. Introduction

Poly(lactic acid), or more correctly, polylactide (PLA), is a bio-based and biodegradable linear aliphatic polyester. Lactic acid, *i.e.*, 2-hydroxypropionic acid, comprises its basic building block, which is in turn derived from the fermentation of starch sources (*e.g.*, corn, potato, sugarcane, tapioca, etc.). To attain high molecular weights (M_w), PLA is habitually prepared by ring-opening polymerization (ROP) of lactide, *i.e.*, the six-membered cyclic diester of lactic acid, using tin octanoate as catalyst (Garlotta, 2001). PLA is nowadays considered the front runner in the emerging bioplastics market, showing an annual consumption of 140,000 tons (Madhavan Nampoothiri et al., 2010). This biopolyester is particularly interesting for short-term applications (*e.g.*, food packaging) due to its two-fold environmental advantage of being obtained from renewable resources, *i.e.* bio-based, and biodegradable, though durable applications can be also possible (Nagarajan et al., 2016). Physical properties of PLA are fairly similar to those of petrochemical-based polymers with high strength and low toughness such as polystyrene (PS) and poly(ethylene terephthalate) (PET) (Auras et al., 2010). Most common uses include disposable and compostable glasses for cold drinks, food trays and rigid containers, teabags, lids, disposable plates, cutlery, etc. (Lim et al., 2008). By using natural fillers (*e.g.*, cellulosic materials) as reinforcement for PLA matrices, fully bio-based and biodegrable composites can be manufactured (Johari et al., 2016; Oksman et al., 2003; Plackett et al., 2003; Yusoff et al., 2016). These constitute the so-called "green composites", which represent an emerging area in materials science and sustainable chemistry (La Mantia and Morreale, 2011).

Almond (*Prunus amygdalus* L.) is a very important crop throughout the world's temperate regions with an annual production of 2.31 million tons from a land area of 1.7 million hectare (Pirayesh et

al., 2013). The almond tree fruit, the drupe, is considered to comprise of four parts, namely, the almond flesh, the almond flesh brown skin, the almond green shell cover (hull), and the almond shell (Esfahlan et al., 2010). The latter constitutes the thick endocarp of the almond fruit that is composed, on a dry basis, of approximately 38 wt.-% of hemicellulose, 31 wt.-% cellulose (Kürschner), 28 wt.-% of lignin (Klason), and 3 wt.-% of other components (Caballero et al., 1997; Martínez et al., 1995). After harvesting, these woody shells are separated to obtain the edible seeds, which are widely employed in the food industry, remaining available as a solid residue for which no relevant industrial use has been developed to date (Esfahlan et al., 2010). Some novel applications of almond shells are being continuously proposed, such as heavy metal adsorbents, dye absorbents, growing media, activated carbon preparation, and additives for the preparation of xylo-oligosaccharides (XOs) (Deniz, 2013; Doulati Ardejani et al., 2008; Ebringerová et al., 2007; Esfahlan et al., 2010; Urrestarazu et al., 2005). However, currently almond shells are mainly incinerated (Chiou et al., 2016) or used as animal feed (Ledbetter, 2008). Additionally, it is worth to note that the processing byproducts, *i.e.*, hulls and shells, account for more than 50% by dry weight of the almond fruit (Fadel, 1999). Consequently, it is estimated that around 0.8–1.7 million tons of this agro-waste are annually generated (Pirayesh and Khazaeian, 2012). As a result, these highly lignified materials are potential candidates to be applied as renewable fillers to reinforce polymer and biopolymer matrices. For this application, the shells are required to be ground and dried to obtain a more easy-to-handle product in a powder form, *i.e.* the almond shell flour (ASF).

Previous studies on green composites based on ASF are not very extensive and these are limited to the use of urea-formaldehyde (UF) resin (Gürü et al., 2006; Pirayesh et al., 2013; Pirayesh and Khazaeian, 2012), epoxy resin (Chaudhary et al., 2013), polypropylene (PP) (Essabir et al., 2013b; Hosseinihashemi et al., 2016; Lashgari, 2013), polyvinyl chloride (PVC) (Crespo et al., 2007a; Crespo et al., 2007b), and poly(ε-caprolactone) (PCL) (Valdés et al., 2016; Valdés García et al., 2014). In relation to thermoplastic materials, these previous studies have shown that the

incorporation of ASF can bring important advantages such as mechanical reinforcement, reduce environmental impact, and lower costs. Besides intrinsic properties of each component, the mechanical and thermomechanical properties of the resultant green composites are dependent on filler aspect ratio, filler content and orientation, and on adhesion at the filler-matrix interface (Nagarajan et al., 2013). The latter, *i.e.*, the interfacial filler-matrix adhesion, is crucial since it is responsible for promoting a good stress transfer from the continuous phase to the dispersed fillers that must carry the load. Nevertheless, the high inherent hydrophilicity of cellulosic fillers does not habitually offer good adhesion with the hydrophobic or low hydrophilic polymers used as the composite matrix (Torres-Giner et al., 2017). Poor filler wetting causes a non-uniform distribution of fillers in the matrix, consequently aggregation and void formation is commonly observed during melt processing. Many different approaches, reported in multiple reviews (Bledzki and Gassan, 1999; Bledzki et al., 1996; La Mantia and Morreale, 2011; Wei and McDonald, 2016), have explored different strategies to improve adhesion in cellulose-reinforced polymer materials. These methods mainly include surface modification of the cellulosic filler prior to composite manufacture *via* chemical (*e.g.*, esterification, etherification, treatment with silanes or isocyanates) or physical means (*e.g.*, plasma, corona treatments, and radiation) as well as modification of the polymer matrix. Among them, the exposure to ultraviolet (UV) radiation has been recently demonstrated to be very effective on the activation of the cellulosic filler surface in order to improve the physical properties of the resultant polymer composites (Torres-Giner et al., 2016b).

An alternative approach to improve filler-matrix adhesion and filler dispersion in polymer composites is the use of a compatibilizer, playing the role of an adhesion promoter (Sengupta et al., 2013). In this sense, reactive extrusion (REX) is a well-known and cost-effective methodology to introduce a variety of functional groups into biopolymer chains (Miladinov and Hanna, 2000; Raquez et al., 2006). Based on this concept, REX has been recently proposed as novel route for grafting inorganic nanoparticles onto biopolymer matrices, resulting in sustainable polymer

nanocomposites with enhanced physical performance (Torres-Giner et al., 2016a). This is due to biopolyester chains are characterized by hydroxyl and carboxylic acid terminal groups, which can establish chemical interactions during melt processing. This process mainly involves the chemical attachment of the fillers to the biopolymer chains by the action of reactive molecules with, on average, two or more functionalities (*f*), *i.e.*, molecules with at least two functional sites. These bi- or multi-functional additives actually act as interfacial agents and improve adhesion between filler and the polymer continuous phase by the creation of covalent bonds.

Maleinized linseed oil (MLO) is a natural crosslinker that is industrially prepared from linseed oil, which is extracted from the seeds of flaxseed (*Linum usitatissimum* L.), a plant widely cultivated in Europe. Linseed oil contains approximately 8-12% saturated (mainly 4-7% palmitic acid and 4-5% stearic acid) and 85-92% unsaturated fatty acids (mainly 50-55% linolenic acid, 20-25% oleic acid, and 12-15% linoleic acid) (Bayrak et al., 2010). This unsaturated fatty acid content results in one of the highest unsaturation levels amongst common vegetable oils, comparable only to tung oil, thus leading to a highly versatile additive, ripe for chemical functionalization. In particular, the maleinization process provides multiple anhydride functionalities to the MLO structure, which could easily react thereafter with hydroxyl groups (Ford et al., 2011; Ford et al., 2012). Moreover, MLO offers an important advantage in comprison to other maleinized oils since it is commercially available at a competitive price due to its alternative uses as biolubricant. Additionally, small amounts of MLO can also act as a sustainable plasticizer for PLA-based materials, allowing chain motion and improving their processing conditions, thermal stability, and ductility (Ferri et al., 2017). Moreover, the use of vegetable oils (VOs) is of great interest from an environmental point of view as these lend themselves to obtaining fully bio-based and compostable formulations (Garcia-Garcia et al., 2016). Based on recent research findings (Ferri et al., 2016), the present study reports the compatibilization by MLO of cellulosic ASF with PLA biopolymer. The influence of different

contents of MLO on the thermal, mechanical, and morphological properties of these novel green composites is evaluated and related to its compatibilizing effect.

2. Materials and methods

2.1. Materials

The PLA used was Ingeo™ Biopolymer 3251D, supplied by NatureWorks (Minnetonka, Minnesota, USA). According to the manufacturer, this is an injection molding-grade resin made primarily from dextrose that is derived from field corn grown for industrial and functional end-uses. The biopolymer has a M_W of 5.5 x 10^4 g/mol, with a polydispersity index (PI) of 1.62, a melt flow rate (MFR) of 30-40 g/10 min (190°C, 2.16 kg), and a true density of 1.24 g/cm³. Almond (*Prunus amygdalus* L.) was collected in the Sierra Mariola region and the shells were provided by Jesol Materias Primas S.A. (Valencia, Spain) as an industrial byproduct after seed extraction. MLO was obtained from Vandeputte (Mouscron, Belgium) as VEOMER LIN. This agent has a viscosity of 1,000 cP at 20°C and an acid value of 105–130 mg potassium hydroxide (KOH)/g.

2.2. Preparation of almond shell flour

The as-received almond shells were ground in a Retsch GmbH (Düsseldorf, Germany) SK 100 Cross Beater mill at a rotating speed of 10,000 rpm. Resultant particles were then sieved using a Cisa® Sieve Shaker model RP09 (Barcelona, Spain) to obtain a flour with a homogenous particle size distribution with a top-cut of 150 μm. **Figure 1** shows the almond shells and the obtained ASF in powder form. Subsequently, ASF was UV irradiated in a Honle UV Technology (Barcelona, Spain) UVASPOT 1000RF2 cabinet for 4 min, based on previous research (Torres-Giner et al., 2016b), using a high pressure mercury lamp with a power of 1,000 W at a wavelength at 350 nm.

Prior to processing and to remove any residual moisture, the biopolymer pellets and ASF were stored at 60ºC for 36 h in an Industrial Marsé (Barcelona, Spain) dehumidifying dryer MD. The final water content of ASF was kept at 1–2%.

2.3. Reactive extrusion

A constant weight percentage of 30 wt.-% of ASF in PLA was selected to evaluate the influence of MLO on the measured physical properties. This composite composition was chosen based on previous reported results observed for other PLA green composites (Balart et al., 2016b). The MLO range composition was subsequently varied in the range of 0–10 parts per hundred resin (phr) since previous studies with other VOs indicated saturation with contents below 10 phr (Balart et al., 2016a). **Table 1** summarizes the set of the prepared green composite formulations.

Extrusion was performed on a twin-screw co-rotating extruder ZSK-18 MEGAlab from Coperion (Stuttgart, Germany). The screws feature 18 mm diameter with a length (L) to diameter (D) ratio, *i.e.*, L/D, of 48. The materials dosage was set to achieve a residence time of about 1 min, measured by a blue masterbatch and based on a previously described configuration (Torres-Giner et al., 2016a). To this end, ASF was fed into a ZS-B 18 twin-screw side feeder from K-Tron (Pitman, New Jersey, USA) while MLO was added through a loss-in-weight (LIW) liquid feeder FDDW-MD2-DKMP-6 from Brabender Technologie GmbH (Duisburg, Germany). The screw speed was fixed at 300 rpm and the temperature profile, from the hopper to die, was set as follows: 170–180–180–180–190–190–190°C. The extruded material was cooled in a water bath at 15°C and pelletized using an air-knife unit.

2.4. Injection molding

Green composite pellets were shaped into pieces by injection molding in a Meteor 270/75 from Mateu & Solé (Barcelona, Spain) prior to characterization. The profile temperature, from the feeding zone to the injection nozzle, was set as follows: 170–175–180–185ºC. A clamping force of 75 tons was applied. The cavity filling and cooling time were set at 1 and 10 s, respectively. Standard samples with a thickness of 4 mm were obtained.

2.5. Scanning Electron Microscopy

The morphology of the ASF particles and fracture surfaces of the green composite pieces after the impact tests were characterized using scanning electron microscope (SEM). An Oxford Instruments Zeiss Ultra 55 (Abingdon, UK) was used and an acceleration voltage of 2 kV was applied. Samples surfaces were coated with a gold-palladium alloy in a Quorum Technologies Ltd EMITECH model SC7620 sputter coater (East Sussex, UK) prior to analysis. ASF sizes were determined using Image J Launcher v 1. 41 and the data presented were based on measurements from a minimum of 50 SEM micrographs.

2.6. Infrared Spectroscopy

Chemical analysis was performed *via* attenuated total reflection–Fourier transform infrared (ATR-FTIR) spectroscopy. Spectra were recorded using a Bruker S.A. Vector 22 (Madrid, Spain) coupled to a PIKE MIRacle™ single reflection diamond ATR accessory (Madison, Wisconsin, USA). Data were collected as the average of ten scans between 4000 and 400 cm^{-1} at a spectral resolution of 4 cm^{-1}.

2.7. Mechanical tests

Injection-molded specimens with a dumbbell shape, a total length of 150 mm, and a cross-section of 10 x 4 mm^2 were tested in a universal test machine ELIB 30 from S.A.E. Ibertest (Madrid, Spain). Tensile tests were performed according to ISO 527. A 5 kN load cell and a cross-head speed of 5 mm/min were employed. Impact strength was tested on unnotched samples in a 1-J Charpy pendulum from Metrotec S.A. (San Sebastián, Spain), as suggested by ISO 179. Shore D hardness was determined in a durometer 676-D model from J. Bot S.A. (Barcelona, Spain) following ISO 868. All specimens were tested in a controlled chamber at room conditions, *i.e.* 23°C and 50 % RH. Six samples for each material were analyzed and averaged.

2.8. Thermal analysis

Thermal transitions of PLA and its green composites were evaluated by differential scanning calorimetry (DSC) using an 821 DSC model from Mettler-Toledo, Inc. (Schwerzenbach, Switzerland). For this, *ca.* 5 mg samples were placed in 40 µl hermetic aluminum sealed pans, previously calibrated with an indium standard. The analysis was performed in a dry reducing atmosphere in which nitrogen flowed at a constant rate of 66 mL/min. Samples were subjected to a two-step regime based on an initial heating step from 30 to 200°C followed by a cooling step down to 0°C at a heating rate of 10 °C/min. The cold crystallization temperature (T_{cc}), melting temperature (T_m), enthalpy of melting (ΔH_m), and cold crystallization (ΔH_{cc}) were obtained from the heating scan while the crystallization temperature from the melt (T_c) and enthalpy of crystallization (ΔH_c) were determined from the cooling scan. The percentage of crystallinity (X_c) in the samples was determined using the following equation:

$$Xc = \left[\frac{\Delta Hm - \Delta Hcc}{\Delta H_m^0 \cdot (1-w)}\right] \cdot 100$$

where ΔH_m^0 = 93.7 J/g is the theoretical enthalpy corresponding to the melting of a 100% crystalline PLA sample (Torres-Giner et al., 2011), while the term 1-*w* represents the PLA weight fraction in the composite.

Thermogravimetric analysis (TGA) was used to evaluate the thermal stability of the materials using a TGA/SDTA 851 thermobalance from Mettler Toledo, Inc. too. The heating program was set from 30 to 650ºC at a heating rate of 20 ºC/min in nitrogen with a constant flow-rate of 66 mL/min. Approximately 10 mg of each sample was used for the measurements. The onset degradation temperature was defined as the temperature at 5% weight loss ($T_{5\%}$) and the maximum rate degradation temperature (T_{deg}) was obtained from the maximum value of the first derivative.

2.9. Thermomechanical tests

Vicat softening point and heat deflection temperature (HDT) of the injection-molded pieces were both measured using a DEFLEX 687-A2 standard Vicat/HDT station from Metrotec S.A. (San

Sebastián, Spain). Vicat softening point was determined following the UNE-EN 727 and ISO 306, in accordance with the B50 method. The protocol involved the placement of specimens in the testing apparatus so that the penetrating needle rested on its surface at least 1 mm from the edge. A load of 50 N was applied to the sample. This was then lowered into an oil bath in which the temperature was raised at a rate of 50 °C/h until the needle penetrated 1 mm. HDT measurements were carried out according to UNE-EN ISO 75-Method A and ASTM D648, heating the medium (oil) at a rate of of 120 °C/h. A specimen of 80 x 10 x 4 mm^3 was loaded in three-point bending mode in the edgewise direction with a distance of 60 cm. The outer stress used for testing was 1.8 MPa and the temperature was increased at 120 °C/h until the sample deflected 0.31 mm.

Dimensional stability was studied by determining the coefficient of linear thermal expansion (CLTE) using a thermomechanical analyzer (TMA) Q400 model from TA Instruments (New Castle, Delaware, USA). The heating program was set between 0 and 140ºC with a constant heating rate of 2 ºC/min and a load of 0.02 N. The test was performed on injection-molded rectangular samples with dimensions of 40 x 10 x 4 mm^3.

3. Results

3.1. Filler morphology

One of the most important adhesion mechanisms in polymer composites is mechanical interlocking, which is influenced by the filler shape. **Figure 2a** shows the morphology of the ASF powder observed by SEM. In this image a rough perimeter can be seen, which can be a consequence of the crushing process due to the high hardness of this type of filler. A closer observation of the filler surface reveals the presence of some voids and granular features. This unusual porous-like structure on the surface of almond shell contributes to its high degree of roughness. A similar morphology was previously reported for PVC-based composites (Crespo et al., 2007a; Crespo et al., 2007b), which was hypothesized to play a significant role in the adhesion with the polymer. The particle size histogram for AHF, determined from the SEM images, is shown in **Figure 2b**. The

predominant particle size was approximately 75 µm. Habitually this is another relevant parameter in the mechanical properties of green composites. Previous studies also reported that mechanical impairment was much more pronounced in systems compromising large almond shell particles, in particular for those particle sizes greater than 150 µm (Crespo et al., 2007a; Crespo et al., 2007b). This effect is related to the arrangement of the fillers within the polymer matrix, which undoubtedly becomes more heterogeneous.

3.2. Chemical properties

Figure 3a shows the FTIR spectra of the ASF powder, MLO liquid, neat PLA, the unmodified PLA/ASF composite, and the PLA/ASF composite containing 2.5 phr MLO.

The main bands of interest within each sample are described as follows. For ASF, the strongest absorption peak ~1032 cm^{-1} is ascribed to the C–O and C–OH stretching vibrations of polysaccharide rings in cellulose (Liu et al., 2009). There is evidence of a broad absorption band between 3600 and 3000 cm^{-1}, which corresponds to the characteristic O–H stretching vibrations of hydrogen bonded of hydroxyl groups (–OH) (Spinacé et al., 2009). Considering that the ASF particles were dried and exposed to UV radiation, these peaks should be mostly derived from –OH on the pyranose rings of cellulose (Lin and Dufresne, 2013), but the presence of small quantities of sorbed water cannot be excluded. The band centered at 1735 cm^{-1} represents the carbonyl (C=O) stretching (Doulati Ardejani et al., 2008). The low intensity bands observed in the range 1400–1300 cm^{-1} are attributed to the bending vibrations of C–H and C–O groups of the polysaccharide ring (Olsson and Salmén, 2004). The absorbance band at ~1234 cm^{-1} corresponds to the C–O–C stretching vibration of the acetyl group in lignin and hemicellulose component, respectively (Doulati Ardejani et al., 2008; Essabir et al., 2013a).

Principal absorption bands for MLO are observed at ~3008 cm^{-1}, which has been identified as the =C–H stretching of the carbon-carbon double bonds, and at ~2924 cm^{-1} and ~2853 cm^{-1} as the antisymmetric and symmetric C–H stretching of the saturated carbon–carbon (C-C) bonds,

respectively (Gomez et al., 2011). Other main bands can be observed at ~1742 cm^{-1} and 1708 cm^{-1}, being associated to the C=O stretching of the carbonyl functionalities from the ester and maleic anhydride groups respectively, at 1161 cm^{-1} for the C–O–C, C–O and C–C stretching to the ester functionalities, and at 719 cm^{-1} to the C–H out of the plane stretching of the saturated C-C bonds (Gomez et al., 2011). The band centered at ~1458 cm^{-1} is ascribed to C–H bending while peaks related to the anhydride groups are seen as shoulders on the ester carbonyl at ~1810 and 1777 cm^{-1}.

One of the strongest peak of neat PLA spectrum appears at 1751 cm^{-1} and is assigned to C=O stretching of the biopolymer (Paragkumar et al., 2006). Other strong bands observed are seen in between 1250–1050 cm^{-1}, which arise from the ester C–O and C–O–C stretching vibrations (Torres-Giner et al., 2011). Bands in the range 1500–1300 cm^{-1} are ascribed to symmetric and antisymmetric deformational vibrations of C–H in the methyl (CH_3) groups (Braun et al., 2006), in which the peak centered at 1450 cm^{-1} is related to C–H bends from lactic acid moieties. The weak bands located at *ca.* 3000 and 2850 cm^{-1} are assigned to the antisymmetric and symmetric stretching vibrations of $–CH_2$ (Braun et al., 2006). Incorporation of ASF certainly disrupted the C–H vibrations (see subtle changes in the regions 3000–2850 and 1500–1300 cm^{-1}) of the biopolymer backbone chain, but it did not produce further significant changes in the spectrum of PLA.

Interestingly, the addition of MLO produced additional changes with regard to the uncompatibilized PLA/ASF composite. One can observe in **Figure 3b** the formation of a shoulder in the carbonyl peak of PLA at approximately 1690 cm^{-1}. This can be related to the C=O stretching group of hydrolyzed anhydride groups of MLO in the green composite (Wu and Su, 1991). There is another weak increased absorption band in the range 1780–1850 cm^{-1} that can be ascribed to the symmetric stretching and asymmetric stretching of C═O of remaining cyclic maleic anhydride (MAH) groups (John et al., 1997; Zhu et al., 2012). The presence of new weak peaks in the region 3600–3300 cm^{-1} can be further attributed to O–H stretch of the newly formed free carboxylic acid and may also indicate the presence of sorbed water in the green composite due to the presence of ASF. This is in

agreement with Eren *et al.* (Eren et al., 2003) who observed a new carbonyl band of the carboxylic acid at 1709 cm^{-1} and a broad carboxylic O–H centered at 3286 cm^{-1} during the polyesterification reaction of diols with maleinized soybean oil (MSO). Additionally, the formation of two new bands at ~1560 and 1518 cm^{-1}, which are most likely to be derived from the antisymmetric stretches of delocalized deprotonated carboxylic acid end groups, can be produced as a result of interaction with sorbed water (Cabaniss et al., 1998). The symmetric stretch of these newly formed functional groups, expected to appear close to 1350 cm^{-1}, are not explicitly visible to permit verification of this hypothesis due to the proximity of C–H band associated with PLA. Nevertheless, it is clear that the incorporation of MLO into the green composite perturbed the band shape at the peak ~1360 cm^{-1} and formation of these delocalized carboxyl groups would readily explain this phenomenon.

These FTIR results suggest that new esters and carboxylic acids were produced after MLO addition to the green composites. The expected chemical reaction of MLO with PLA biopolymer and the cellulose component of ASF is given in **Figure 4**. This scheme proposes that carboxylic ester linkages are formed upon elevated temperature during melt processing. The MLO structure provides multiple chemical reaction sites, by the presence of a various number of MAH groups, giving therefore reliable bond strength for hydroxyl groups of both the PLA end chains (and partially hydrolyzed PLA chains) and ASF surface. As a result of the esterification reaction, a cellulose-grafted PLA (cellulose-*g*-PLA) structure was generated.

3.3. Mechanical properties of green composites

Figure 5 summarizes the mechanical properties of the neat PLA and its green composites with varying the MLO content. Unreinforced PLA displayed a tensile modulus and strength of 1960 and 63 MPa, respectively (**Figure 5a** and **5b**). In addition, Shore D hardness was ~79.6 (**Figure 5e**). These values indicate that PLA is intrinsically an elastic and rigid material. Nevertheless, PLA is also brittle, showing a low elongation-at-break value of 5.3% and poor energy absorption with an impact-strength value of 15.7 kJ/m^2 (**Figures 5c** and **5d**). Filling PLA with 30 wt.-% ASF led to a

considerable decrease in mechanical properties, particularly for those related to material cohesion such as tensile strength, elongation at break, and impact strength. In particular, tensile modulus and strength were reduced to 1520 and 18 MPa, respectively (**Figures 5a** and **5b**). Elongation at break was also reduced to 2.5% and impact strength to 7 kJ/m^2 (**Figures 5c** and **5d**), which represents an overall percentage reduction of approximately 55% in the mechanical ductility with regard to unfilled PLA. As a positive effect, the filler addition contributed to a slight increase in Shore D hardness to a value of 84.7, *i.e.*, about 7% (**Figure 5e**). Similar mechanical results have been observed recently for other PLA-based green composites in which impact absorbed energy was reduced by about 40% and Shore D hardness increased 9% by the presence of 30 wt.-% of hazelnut shell flour (HSF) (Balart et al., 2016b). Here, the reported results clearly confirm the lack of compatibility between the PLA matrix and ASF.

As an efficient plasticizer, MLO remarkably improved the ductility of the green composites. Elongation-at-break values gradually increased up to 9.8%, for the green composites containing 5 phr MLO, *i.e.* an increase of about 292% and 84% in relation to the uncompatibilized green composite and to the neat PLA, respectively (**Figure 5c**). This is due to the strong plasticization effect provided by MLO on the PLA matrix, where the molecules place among the biopolymer chains acting as a lubricant with an enhanced influence on chain mobility (Chieng et al., 2014). Additionally, MLO could move into the free volume of the green composite, improving its impact-absorbed energy. As a result, incorporation of 5 phr MLO increased the impact-strength value up to 12.1 kJ/m^2 (**Figure 5d**), which represents a percentage increase of about 73% with regard to unmodified green composite. In relation to the Shore D hardness, green composites with MLO contents of 2.5 and 5 phr presented similar values than the unmodified composite, *i.e.* 84.4 and 83.9, respectively, which can be regarded as a positive effect too (**Figure 5e**). However, for the green composites with the highest MLO contents, *i.e.* 7.5 and 10 phr, it was observed an overall decrease in the mechanical properties. This indicates that saturation occurred from 7.5 phr MLO, resulting in a phase separation in the green composites (Ferri et al., 2016).

Both the increase in elongation at break and impact strength indicate that the addition of MLO led to more ductile green composites, which can be explained by the previously described plasticization effect. However, interestingly, the addition of MLO in the range of 1–5 phr MLO also resulted in a noticeable increase in the tensile strength of the green composites. For instance, incorporation of 2.5 phr MLO showed a tensile strength value of 40.1 MPa (**Figure 5b**), which represents an increase of 118% in comparison to the uncompatibilized green composite. For contents over 7.5 phr MLO, a clear decrease in both mechanical strength and ductility was observed. This negative effect can be related to the above-described phase separation of the VO in the green composite due to an excess of concentration. This suggests that an optimal and balanced performance from a mechanical perspective is achieved for MLO contents close to 5 phr. Here, the reported improvement of both mechanical strength and ductility gives some evidences that, in addition to plasticization, a degree of grafting occurred. This supports the previously described infrared data of the MLO-treated green composites in which ester bonds are potentially formed between the multiple MAH groups present in MLO with the hydroxyl groups of both PLA and ASF. This successfully induced an effective stress transfer from the biopolymer to the reinforcing fillers.

3.4. Thermal properties of green composites

Table 2 shows a summary of the main thermal parameters obtained from DSC and TGA for PLA and its green composites treated with different amounts of MLO. As it can be seen in the table, PLA was characterized by a T_g of ~67ºC, a T_m of 172ºC, and a X_c of ~15%. In addition, the biopolymer showed cold crystallization phenomenon with a T_{cc} of approximately 111ºC. After ASF incorporation, the value of T_m was reduced to 168.5ºC and crystallinity also decreased to ~9%. These results indicate that the presence of ASF can potentially disrupt the folding process of PLA chains, which avoids the formation of more perfect crystals and supports the findings from the infrared data. Although Hosseinihashemi *et al.* (Hosseinihashemi et al., 2016) have recently reported that almond shell particles are capable of acting as a nucleating agent that is able to

increase T_c of the resultant polymer composites, ASF could also interfere with the growing stage by which the overall crystallinity level of the composite decreased.

For the MLO-treated green composites, the addition of MLO increased X_c and also, interestingly, induced a significant reduction in T_{cc}. It is important to remark that only the addition of 1 phr MLO led to a significant decrease in T_{cc} of approximately 12ºC and a value of X_c of ~23%. The presence of MLO in the green composites improved the compatibilization and subsequently the dispersion of ASF in the PLA matrix, which contributes to fewer polymer–polymer interactions and favors the formation of PLA crystals (Chieng et al., 2014). In addition, as described previously, MLO can readily react with hydroxyl groups in both PLA end chains and the cellulosic surface of ASF, leading to a combined effect of grafting and chain extension. Alternatively, as expected, T_g decreased as a function of the MLO content. This is related to an overall increase in the PLA chain mobility. It can be considered that MLO, due to its low M_w as well as good chemical affinity with the biopolymer, facilitates the reduction of secondary forces (*e.g.* hydrogen bonding, van der Waals forces, etc.) among the PLA chains by occupying intermolecular spaces and increasing the free volume.

As also included in **Table 2**, the evaluation of thermal stability of the unmodified green composite showed a downward shift in T_{deg} from 339.3ºC, for the neat PLA, to 308.6ºC, for the untreated PLA/ASF composite. The unmodified green composite also began to degrade at a lower temperature, of around 5ºC, *i.e.* a $T_{5\%}$ of approximately 290ºC. Therefore, a significant decrease in the thermal stability of PLA was clearly noticeable after the incorporation of ASF. This fact is related to the relatively low thermal stability of the lignocellulosic filler, which initiated degradation at 221.2ºC and, one assumes, negatively contributed to the reduction of the global thermal stability of the green composite. In the present study, the observed impairment is in agreement with previous studies concerning the thermal stability of polymer composites based on almond shell (Essabir et al., 2013b; Hosseinihashemi et al., 2016; Valdés García et al., 2014). It was specifically reported

that the degradation of these natural fillers initially occurs in the range 250–350ºC, which is assigned to the thermal decomposition of cellulose and lignin (Hosseinihashemi et al., 2016). Interestingly, the addition of MLO exerted a positive effect on the overall thermal stability of the green composites. Specifically, the onset degradation temperature, corresponding to 5% weight loss, increased to values in the range of 305–300ºC for the green composites compatibilized by MLO. Thermal degradation was also significantly improved in comparison to the unmodified green composite. In particular, T_{deg} was delayed up to about 20ºC for the green composites treated with MLO. This remarkable increase in the thermal stability can be directly related to the chemical interaction achieved by MLO due to the covalent bonds established between the lignocellulosic fillers and the biopolymer matrix. In addition, MLO could also provide a physical barrier that obstructs the removal of volatile products produced during decomposition. A similar positive effect on the thermal stability was recently reported for PLA and epoxidized palm oil (EPO) blends (Chieng et al., 2014; Silverajah et al., 2012). Indeed, Chieng *et al.* (Chieng et al., 2014) observed a remarkable increase of 40°C in the onset degradation of PLA by incorporating 5 wt.-% EPO.

3.5. Thermomechanical properties of green composites

Table 3 shows the values of Vicat softening temperature, HDT, and CLTE, which are representative parameters for the thermomechanical properties of the green composites. With regard to the Vicat softening temperature, the value of unfilled PLA was 56.2ºC and this increased to 73.4ºC after the addition of 30 wt.-% ASF. This is in agreement with previous studies conducted on PLA/HSF composites (Balart et al., 2016b). Interestingly, the incorporation of MLO also showed a considerable increase in the softening point, reaching a maximum value of 87.3ºC. This represents an increase of about 55% in relation to the unfilled PLA, further supporting the chemical interaction of ASF with the biopolymer. It is also worthy to indicate that the highest value was observed for the green composites containing 1 phr MLO, which further confirms that higher MLO amounts plasticize the PLA matrix and therefore reduce the service temperature of the green composites. A

similar trend was also observed for HDT, in which the highest value was attained for the green composites containing 2.5 phr MLO. In particular, HDT increased from 53.1 and 61.6 ºC for the neat PLA and unmodified green composite, respectively, up to 63.6 ºC.

The effect of compatibilization of MLO on the green composites was additionally determined by TMA. **Table 3** also includes the CLTE values, below and above T_g, which are indicative of the dimensional stability of the green composites. As it can be seen in the table, the linear expansion was lower in the range of temperatures below T_g, which are ascribed to restrictions in the biopolymer chain mobility. Comparison of CLTE values below T_g shows that the incorporation of ASF reduced them from 79.1 to 64.4 µm/mºC. This indicates that ASF successfully reinforced the PLA matrix and improved the dimensional stability of the biopolymer, producing analogous findings to those recently described for PLA/HSF composites (Balart et al., 2016b). With regard to the evolution of the CLTE values in the compatibilized green composites, these increased with increasing the MLO content and ranged from about 63 to 81 µm/mºC. This can be explained by the plasticization effect provided by MLO, which facilitates the PLA chains mobility and increases free volume. The evolution of the CLTE values over T_g followed a similar tendency, showing a significant increase from 116.4 µm/mºC, for the unmodified green composite, up to 152.6 µm/mºC for the green composite containing 10 phr MLO. Plasticization was then more pronounced at higher temperatures, which is in agreement with previously studies looking at PLA-based green composites plasticized by epoxidized linseed oil (ELO) (Balart et al., 2016a). All green composites showed higher dimensional stability than the neat PLA. This can be considered as a positive finding, facilitating the technical applications of PLA materials at elevated temperatures.

3.6. Morphology of green composites

Figure 6 shows the SEM images of the fracture surfaces of PLA and its green composites after the impact tests. **Figure 6a**, which corresponds to the uncompatibilized PLA/ASF composite, clearly illustrates the typical brittle fracture of the biopolymer showing a rough fracture surface due to

nonexistent or very low plastic deformation. In addition, the lack of interaction between ASF and PLA was clearly detectable by the presence of several voids, which correspond to the detached particles after impact. Interestingly, some of the voids also showed the marks of the AHF surface. This supports a recent finding in which it was indicated that particle debonding was the main failure mechanism of cellulosic fillers in biopolymer matrices (Torres-Giner et al., 2017). This occurs due to the lack of adhesion or cohesion at the particle–matrix interface of the green composite. This morphological observation correlates satisfactorily with the above-described physical performance of the unmodified green composites in which the presence of ASF did not contribute to an improvement of the mechanical and thermal properties but it rather decreased them.

The positive effect of MLO addition on the morphology of the green composite can be seen in **Figures 6b** to **6f**. Although it is possible to still detect some voids in the PLA matrix after the addition of 1 phr MLO (**Figure 6b**), the presence of finely dispersed AHF particles into PLA indicates that MLO certainly improved compatibility. The addition of 2.5 phr (**Figure 6c**) and 5 phr MLO (**Figure 6d**) clearly led to an improvement of the particle–polymer continuity, which is subsequently responsible for reducing stress concentration phenomena and increasing load transfer between the biopolymer matrix and the lignocellulosic filler. One can also observe that as the MLO content increased, the filler-matrix gap was reduced. **Figure 6e** shows the good dispersion of the ASF particles within the PLA matrix containing 7.5 phr MLO. This image supports the hypothesis that the presence of MLO in the green composites improved ASF wettability. This can be confirmed by **Figure 6f** for the PLA/ASF composite containing 10 phr MLO in which the lignocellulosic fillers were completely covered by MLO. It can be also observed the absence of gaps with the surrounding PLA, which points towards improved interfacial affinity. However, certain phase separation was also detectable due to the MLO saturation, which is in turn considered to be responsible for impairing the performance of the green composites.

4. Conclusions

The present study described the compatibilization of PLA and ASF by the addition of MLO during melt compounding. It was observed that the incorporation of high amounts of ASF into PLA resulted in green composites with increased hardness and potentially offers a remarkable cost reduction and improved waste valorization. However, it considerably reduced ductility and also thermal stability. Interestingly, addition of relatively low contents of MLO, *i.e.* 1–5 phr, successfully improved the mechanical, thermal, and thermomechanical properties of the green composites. The achieved compatibilization was ascribed to a dual effect of plasticization and grafting provided by MLO. As supported by FTIR analysis, new ester bonds were potentially formed during the extrusion process between the multiple MAH groups of MLO with the hydroxyl groups present on the ASF surface and PLA terminal chains. For PLA/ASF composites containing high MLO amounts, *i.e.* 7.5 and 10 phr, an overall decrease in the physical properties occurred probably due to plasticizer saturation.

The results obtained in this study indicate that ASF, derived as a byproduct from the food industry, can be used to reinforce PLA matrices when combined with low amounts of MLO due to its multi-functional reactivity. Moreover, the resultant MLO-containing green composites are highly sustainable because of their completely biodegradable and renewable characteristics. These can be applied as monolayers, in bio-based packaging materials, such as trays and lids, or even as replacements for wood boards or docks in building and construction applications.

In general terms, MLO and other multi-functionalized vegetable oils can be regarded as an attractive additive to enhance compatibility in immiscible or low miscible green composites based on biopolymers and fillers with polar groups. In addition, due to their natural origin, MLO represents an environmentally friendly solution to improve industrial formulations and can positively contribute to the development of sustainable polymer technologies.

Acknowledgements

This research was supported by the Ministry of Economy and Competitiveness (MINECO) program number MAT2014-59242-C2-1-R and AGL2015-63855-C2-1-R and Generalitat Valenciana (GV) program number GV/2014/008. L. Quiles-Carrillo wants to thank GV for financial support through a FPI grant (ACIF/2016/182) and the Spanish Ministry of Education, Culture, and Sports (MECD) for his FPU grant (FPU15/03812).

References

Auras, R., Lim, L.-T., Selke, S.E.M., Tsuji, H., 2010. Poly(Lactic Acid): Synthesis, Structures, Properties, Processing, and Applications, in: Rafael Auras, L.-T.L., Susan E. M. Selke, Hideto Tsuji (Ed.). John Wiley & Sons, Inc., Hoboken, New Jersey.

Balart, J.F., Fombuena, V., Fenollar, O., Boronat, T., Sánchez-Nacher, L., 2016a. Processing and characterization of high environmental efficiency composites based on PLA and hazelnut shell flour (HSF) with biobased plasticizers derived from epoxidized linseed oil (ELO). Composites Part B: Engineering 86, 168-177.

Balart, J.F., García-Sanoguera, D., Balart, R., Boronat, T., Sánchez-Nacher, L., 2016b. Manufacturing and properties of biobased thermoplastic composites from poly(lactid acid) and hazelnut shell wastes. Polymer Composites DOI: 10.1002/pc.24007.

Bayrak, A., Kiralan, M., Ipek, A., Arslan, N., Cosge, B., Khawar, K.M., 2010. Fatty Acid Compositions of Linseed (Linum Usitatissimum L.) Genotypes of Different Origin Cultivated in Turkey. Biotechnology & Biotechnological Equipment 24, 1836-1842.

Bledzki, A.K., Gassan, J., 1999. Composites reinforced with cellulose based fibres. Progress in Polymer Science 24, 221-274.

Bledzki, A.K., Reihmane, S., Gassan, J., 1996. Properties and modification methods for vegetable fibers for natural fiber composites. Journal of Applied Polymer Science 59, 1329-1336.

Braun, B., Dorgan, J.R., Dec, S.F., 2006. Infrared Spectroscopic Determination of Lactide Concentration in Polylactide: An Improved Methodology. Macromolecules 39, 9302-9310.

Caballero, J.A., Conesa, J.A., Font, R., Marcilla, A., 1997. Pyrolysis kinetics of almond shells and olive stones considering their organic fractions. Journal of Analytical and Applied Pyrolysis 42, 159-175.

Cabaniss, S.E., Leenheer, J.A., McVey, I.F., 1998. Aqueous infrared carboxylate absorbances: aliphatic di-acids. Spectrochimica Acta Part A: Molecular and Biomolecular Spectroscopy 54, 449-458.

Chaudhary, A.K., Gope, P.C., Singh, V.K., 2013. Effect of Almond Shell Particles on Tensile Property of Particleboard. Journal of Materials and Environmental Science 4, 109-112.

Chieng, B.W., Ibrahim, N.A., Then, Y.Y., Loo, Y.Y., 2014. Epoxidized vegetable oils plasticized poly(lactic acid) biocomposites: mechanical, thermal and morphology properties. Molecules 19, 16024-16038.

Chiou, B.-S., Valenzuela-Medina, D., Bilbao-Sainz, C., Klamczynski, A.P., Avena-Bustillos, R.J., Milczarek, R.R., Du, W.-X., Glenn, G.M., Orts, W.J., 2016. Torrefaction of almond shells: Effects of torrefaction conditions on properties of solid and condensate products. Industrial Crops and Products 86, 40-48.

Crespo, J.E., Balart, R., Sanchez, L., Lopez, J., 2007a. Mechanical behaviour of vinyl plastisols with cellulosic fillers. Analysis of the interface between particles and matrices. International Journal of Adhesion and Adhesives 27, 422-428.

Crespo, J.E., Sanchez, L., Parres, F., López, J., 2007b. Mechanical and morphological characterization of PVC plastisol composites with almond husk fillers. Polymer Composites 28, 71-77.

Deniz, F., 2013. Dye removal by almond shell residues: Studies on biosorption performance and process design. Materials Science and Engineering: C 33, 2821-2826.

Doulati Ardejani, F., Badii, K., Limaee, N.Y., Shafaei, S.Z., Mirhabibi, A.R., 2008. Adsorption of Direct Red 80 dye from aqueous solution onto almond shells: Effect of pH, initial concentration and shell type. Journal of Hazardous Materials 151, 730-737.

Ebringerová, A., Hromádková, Z., Košťálová, Z., Sasinková, V., 2007. Chemical valorization of agricultural by-products: isolation and characterization of xylan-based antioxidants from almond shell biomass. BioResources 3, 60-70.

Eren, T., Küsefoğlu, S.H., Wool, R., 2003. Polymerization of maleic anhydride–modified plant oils with polyols. Journal of Applied Polymer Science 90, 197-202.

Esfahlan, A.J., Jamei, R., Esfahlan, R.J., 2010. The importance of almond (Prunus amygdalus L.) and its by-products. Food Chemistry 120, 349-360.

Essabir, H., Hilali, E., Elgharad, A., El Minor, H., Imad, A., Elamraoui, A., Al Gaoudi, O., 2013a. Mechanical and thermal properties of bio-composites based on polypropylene reinforced with Nut-shells of Argan particles. Materials and Design 49, 442-448.

Essabir, H., Nekhlaoui, S., Malha, M., Bensalah, M.O., Arrakhiz, F.Z., Qaiss, A., Bouhfid, R., 2013b. Bio-composites based on polypropylene reinforced with Almond Shells particles: Mechanical and thermal properties. Materials and Design 51, 225-230.

Fadel, J.G., 1999. Quantitative analyses of selected plant by-product feedstuffs, a global perspective. Animal Feed Science and Technology 79, 255-268.

Ferri, J.M., Garcia-Garcia, D., Montanes, N., Fenollar, O., Balart, R., 2017. The effect of maleinized linseed oil as biobased plasticizer in poly(lactic acid)-based formulations. Polymer International DOI: 10.1002/pi.5329.

Ferri, J.M., Garcia-Garcia, D., Sánchez-Nacher, L., Fenollar, O., Balart, R., 2016. The effect of maleinized linseed oil (MLO) on mechanical performance of poly(lactic acid)-thermoplastic starch (PLA-TPS) blends. Carbohydrate Polymers 147, 60-68.

Ford, E.N.J., Mendon, S.K., Rawlins, J.W., Thames, S.F., 2011. Spectroscopic analysis of cotton treated with neutralized maleinized soybean oil. Journal of the American Oil Chemists' Society 88, 681-687.

Ford, E.N.J., Rawlins, J.W., Mendon, S.K., Thames, S.F., 2012. Effect of acid value on the esterification mechanism of maleinized soybean oil with cotton. Journal of Coatings Technology Research 9, 637-641.

Garcia-Garcia, D., Fenollar, O., Fombuena, V., Lopez-Martinez, J., Balart, R., 2016. Improvement of Mechanical Ductile Properties of Poly(3-hydroxybutyrate) by Using Vegetable Oil Derivatives. Macromolecular Materials and Engineering, DOI: 10.1002/mame.201600330.

Garlotta, D., 2001. A Literature Review of Poly(Lactic Acid). Journal of Polymers and the Environment 9, 63-84.

Gomez, N.A., Abonia, R., Cadavid, H., Vargas, I.H., 2011. Chemical and spectroscopic characterization of a vegetable oil used as dielectric coolant in distribution transformers. Journal of the Brazilian Chemical Society 22, 2292-2303.

Gürü, M., Tekeli, S., Bilici, İ., 2006. Manufacturing of urea–formaldehyde-based composite particleboard from almond shell. Materials and Design 27, 1148-1151.

Hosseinihashemi, S.K., Eshghi, A., Ayrilmis, N., Khademieslam, H., 2016. Thermal analysis and morphological characterization of thermoplastic composites filled with almond shell flour/montmorillonite. BioResources 11, 6768-6779.

Johari, A.P., Mohanty, S., Kurmvanshi, S.K., Nayak, S.K., 2016. Influence of Different Treated Cellulose Fibers on the Mechanical and Thermal Properties of Poly(lactic acid). ACS Sustainable Chem. Eng. 4, 1619-1629.

John, J., Tang, J., Yang, Z., Bhattacharya, M., 1997. Synthesis and characterization of anhydride-functional polycaprolactone. Journal of Polymer Science Part A: Polymer Chemistry 35, 1139-1148.

La Mantia, F.P., Morreale, M., 2011. Green composites: A brief review. Composites Part A: Applied Science and Manufacturing 42, 579-588.

Lashgari, A.E., Ayoub; Farsi, Mohammad, 2013. A Study on Some Properties of Polypropylene Based Nanocomposites Made Using Almond Shell Flour and Organoclay. Asian Journal of Chemistry 25, 1043-1049.

Ledbetter, C.A., 2008. Shell cracking strength in almond (Prunus dulcis [Mill.] D.A. Webb.) and its implication in uses as a value-added product. Bioresource Technology 99, 5567-5573.

Lim, L.T., Auras, R., Rubino, M., 2008. Processing technologies for poly(lactic acid). Progress in Polymer Science 33, 820-852.

Lin, N., Dufresne, A., 2013. Supramolecular Hydrogels from In Situ Host–Guest Inclusion between Chemically Modified Cellulose Nanocrystals and Cyclodextrin. Biomacromolecules 14, 871-880.

Liu, D., Han, G., Huang, J., Zhang, Y., 2009. Composition and structure study of natural Nelumbo nucifera fiber. Carbohydrate Polymers 75, 39-43.

Madhavan Nampoothiri, K., Nair, N.R., John, R.P., 2010. An overview of the recent developments in polylactide (PLA) research. Bioresource Technology 101, 8493-8501.

Martínez, J.M., Granado, J.M., Montané, D., Salvadó, J., Farriol, X., 1995. Fractionation of residual lignocellulosics by dilute-acid prehydrolysis and alkaline extraction: Application to almond shells. Bioresource Technology 52, 59-67.

Miladinov, V.D., Hanna, M.A., 2000. Starch esterification by reactive extrusion. Industrial Crops and Products 11, 51-57.

Nagarajan, V., Mohanty, A.K., Misra, M., 2013. Sustainable Green Composites: Value Addition to Agricultural Residues and Perennial Grasses. ACS Sustainable Chem. Eng. 1, 325-333.

Nagarajan, V., Mohanty, A.K., Misra, M., 2016. Perspective on Polylactic Acid (PLA) based Sustainable Materials for Durable Applications: Focus on Toughness and Heat Resistance. ACS Sustainable Chem. Eng. 4, 2899-2916.

Oksman, K., Skrifvars, M., Selin, J.F., 2003. Natural fibres as reinforcement in polylactic acid (PLA) composites. Composites Science and Technology 63, 1317-1324.

Olsson, A.-M., Salmén, L., 2004. The association of water to cellulose and hemicellulose in paper examined by FTIR spectroscopy. Carbohydrate Research 339, 813-818.

Paragkumar, N.T., Edith, D., Six, J.L., 2006. Surface characteristics of PLA and PLGA films. Applied Surface Science 253, 2758-2764.

Pirayesh, H., Khanjanzadeh, H., Salari, A., 2013. Effect of using walnut/almond shells on the physical, mechanical properties and formaldehyde emission of particleboard. Composites Part B: Engineering 45, 858-863.

Pirayesh, H., Khazaeian, A., 2012. Using almond (Prunus amygdalus L.) shell as a bio-waste resource in wood based composite. Composites Part B: Engineering 43, 1475-1479.

Plackett, D., Løgstrup Andersen, T., Batsberg Pedersen, W., Nielsen, L., 2003. Biodegradable composites based on L-polylactide and jute fibres. Composites Science and Technology 63, 1287-1296.

Raquez, J.-M., Degée, P., Nabar, Y., Narayan, R., Dubois, P., 2006. Biodegradable materials by reactive extrusion: from catalyzed polymerization to functionalization and blend compatibilization. Comptes Rendus Chimie 9, 1370-1379.

Sengupta, S., Ray, D., Mukhopadhyay, A., 2013. Sustainable Materials: Value-Added Composites from Recycled Polypropylene and Fly Ash Using a Green Coupling Agent. ACS Sustainable Chem. Eng. 1, 574-584.

Silverajah, V.S.G., Ibrahim, N.A., Zainuddin, N., Yunus, W.M.Z.W., Hassan, H.A., 2012. Mechanical, Thermal and Morphological Properties of Poly(lactic acid)/Epoxidized Palm Olein Blend. Molecules 17, 11729.

Spinacé, M.A.S., Lambert, C.S., Fermoselli, K.K.G., De Paoli, M.-A., 2009. Characterization of lignocellulosic curaua fibres. Carbohydrate Polymers 77, 47-53.

Torres-Giner, S., Gimeno-Alcañiz, J.V., Ocio, M.J., Lagaron, J.M., 2011. Optimization of electrospun polylactide-based ultrathin fibers for osteoconductive bone scaffolds. Journal of Applied Polymer Science 122, 914-925.

Torres-Giner, S., Montanes, N., Boronat, T., Quiles-Carrillo, L., Balart, R., 2016a. Melt grafting of sepiolite nanoclay onto poly(3-hydroxybutyrate-co-4-hydroxybutyrate) by reactive extrusion with multi-functional epoxy-based styrene-acrylic oligomer. European Polymer Journal 84, 693-707.

Torres-Giner, S., Montanes, N., Fenollar, O., García-Sanoguera, D., Balart, R., 2016b. Development and optimization of renewable vinyl plastisol/wood flour composites exposed to ultraviolet radiation. Materials and Design 108, 648-658.

Torres-Giner, S., Montanes, N., Fombuena, V., Boronat, T., Sánchez-Nacher, L., 2017. Preparation and characterization of compression-molded green composite sheets made of poly(3-hydroxybutyrate) reinforced with long pita fibers. Advances in Polymer Technology DOI: 10.1002/adv.21789.

Urrestarazu, M., Martínez, G.A., Salas, M.d.C., 2005. Almond shell waste: possible local rockwool substitute in soilless crop culture. Scientia Horticulturae 103, 453-460.

Valdés, A., Fenollar, O., Beltrán, A., Balart, R., Fortunati, E., Kenny, J.M., Garrigós, M.C., 2016. Characterization and enzymatic degradation study of poly(ε-caprolactone)-based biocomposites from almond agricultural by-products. Polymer Degradation and Stability 132, 181-190.

Valdés García, A., Ramos Santonja, M., Sanahuja, A.B., Del Carmen Garrigós Selva, M., 2014. Characterization and degradation characteristics of poly(ε-caprolactone)-based composites reinforced with almond skin residues. Polymer Degradation and Stability 108, 269-279.

Wei, L., McDonald, A.G., 2016. A review on grafting of biofibers for biocomposites. Materials 9.

Wu, C.H., Su, A.C., 1991. Functionalization of ethylene-propylene rubber via melt mixing. Polymer Engineering & Science 31, 1629-1636.

Yusoff, R.B., Takagi, H., Nakagaito, A.N., 2016. Tensile and flexural properties of polylactic acid-based hybrid green composites reinforced by kenaf, bamboo and coir fibers. Industrial Crops and Products 94, 562-573.

Zhu, R., Liu, H., Zhang, J., 2012. Compatibilizing Effects of Maleated Poly(lactic acid) (PLA) on Properties of PLA/Soy Protein Composites. Industrial & Engineering Chemistry Research 51, 7786-7792.

Table 1. Summary of weight compositions (wt.-%) according to the content of polylactide (PLA), almond shell flour (ASF), and maleinized linseed oil (MLO). MLO was added as parts per hundred resin (phr) of PLA/AHF composite.

Samples	Percentage (wt.-%)		MLO (phr)
	PLA	ASF	
PLA	100	-	-
PLA/ASF	70	30	-
PLA/ASF + MLO 1 phr	70	30	1.0
PLA/ASF + MLO 2.5 phr	70	30	2.5
PLA/ASF + MLO 5 phr	70	30	5.0
PLA/ASF + MLO 7.5 phr	70	30	7.5
PLA/ASF + MLO 10 phr	70	30	10.0

Table 2. Thermal properties of polylactide (PLA) and its green composites with almond shell flour (ASF) with varying amounts of maleinized linseed oil (MLO). MLO content is expressed as parts per hundred resin (phr) of PLA/AHF composite. The glass transition temperature (T_g), cold crystallization temperature (T_{cc}), melting temperature (T_m), normalized cold crystallization (ΔH_{cc}), and normalized enthalpy of melting (ΔH_m) are obtained from differential scanning calorimetry (DSC) curves during the second heating scan. The onset degradation temperature, defined as the temperature at 5% weight loss ($T_{5\%}$), degradation temperature (T_{deg}), and residual mass are obtained from the thermogravimetric analysis (TGA) curves. Residual mass is measured at 650ºC.

Samples	**DSC parameters**						**TGA parameters**		
	T_g (ºC)	**T_{cc} (ºC)**	**T_m (ºC)**	**ΔH_{cc} (J/g)**	**ΔH_m (J/g)**	**X_c (%)**	**$T_{5\%}$ (ºC)**	**T_{deg} (ºC)**	**Residual mass (%)**
AHF	-	-	-	-	-	-	221.2 ± 0.3	259.2 ± 0.5	1.1 ± 0.2
PLA	66.7 ± 0.3	111.3 ± 0.3	172.1 ± 0.4	21.1 ± 0.3	35.1 ± 0.3	14.9 ± 0.3	295.0 ± 0.5	339.3 ± 0.5	0.5 ± 0.2
PLA/ASF	58.1 ± 0.3	110.1 ± 0.1	168.5 ± 0.5	22.6 ± 0.3	28.6 ± 0.3	9.1 ± 0.2	289.8 ± 0.4	308.6 ± 0.4	0.8 ± 0.3
PLA/ASF + MLO 1 phr	62.1 ± 0.2	96.9 ± 0.3	171.4 ± 0.4	17.1 ± 0.2	31.9 ± 0.3	22.8 ± 0.3	299.3 ± 0.5	322.1 ± 0.3	0.6 ± 0.3
PLA/ASF + MLO 2.5 phr	59.9 ± 0.5	103.6 ± 0.3	172.2 ± 0.3	17.3 ± 0.4	30.2 ± 0.2	20.2 ± 0.3	300.6 ± 0.4	322.2 ± 0.4	0.7 ± 0.2
PLA/ASF + MLO 5 phr	58.7 ± 0.3	106.7 ± 0.5	171.9 ± 0.3	18.1 ± 0.3	29.7 ± 0.4	18.6 ± 0.2	301.2 ± 0.5	323.3 ± 0.5	0.6 ± 0.3
PLA/ASF + MLO 7.5 phr	55.2 ± 0.2	103.4 ± 0.4	171.9 ± 0.4	19.9 ± 0.2	27.5 ± 0.3	12.5 ± 0.3	302.2 ± 0.4	325.2 ± 0.2	0.7 ± 0.3
PLA/ASF + MLO 10 phr	54.9 ± 0.3	102.9 ± 0.3	172.3 ± 0.3	20.1 ± 0.2	27.4 ± 0.2	12.4 ± 0.2	304.3 ± 0.3	327.1 ± 0.3	0.7 ± 0.2

Table 3. Vicat softening point, heat deflection temperature (HDT), and coefficient of linear thermal expansion (CLTE) below and above glass transition temperature (T_g) for green composites of polylactide (PLA) with almond shell flour (ASF) with varying amounts of maleinized linseed oil (MLO). MLO content is expressed as parts per hundred resin (phr) of PLA/AHF composite.

Sample	**Vicat (ºC)**	**HDT (ºC)**	**CLTE below T_g (μm/mºC)**	**CLTE above T_g (μm/mºC)**
PLA	56.2 ± 1.9	53.1 ± 1.0	79.1 ± 1.9	170.9 ± 1.9
PLA/ASF	73.4 ± 1.2	61.6 ± 0.4	64.4 ± 1.9	116.4 ± 1.9
PLA/ASF + MLO 1 phr	87.3 ± 1.8	62.7 ± 2.3	63.3 ± 1.9	145.9 ± 1.9
PLA/ASF + MLO 2.5 phr	86.2 ± 0.8	63.6 ± 2.5	72.4 ± 1.9	146.8 ± 1.9
PLA/ASF + MLO 5 phr	81.9 ± 1.8	62.3 ± 1.8	73.8 ± 1.9	149.3 ± 1.9
PLA/ASF + MLO 7.5 phr	81.2 ± 0.4	61.3 ± 1.9	79.8 ± 1.9	151.1 ± 1.9
PLA/ASF + MLO 10 phr	81.3 ± 2.9	62.0 ± 1.6	81.0 ± 1.9	152.6 ± 1.9

Figures.

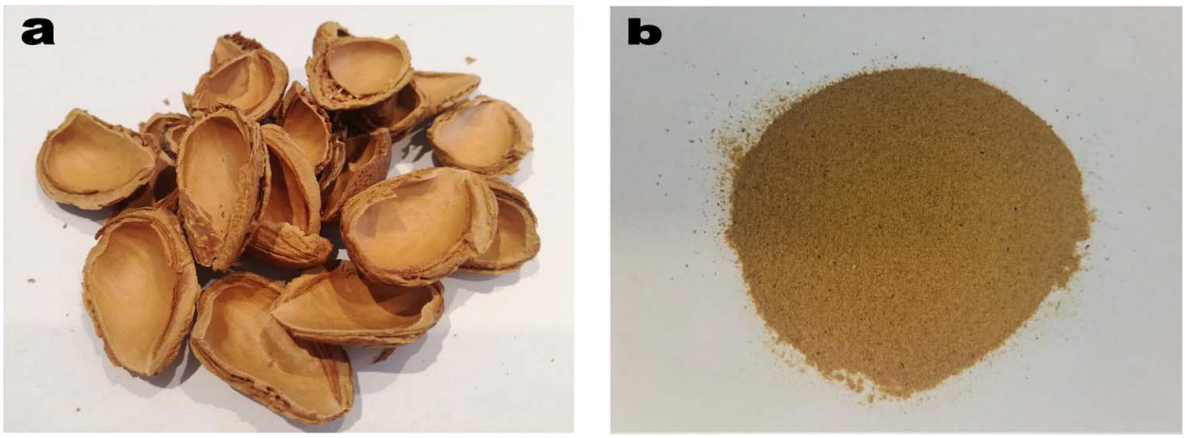

Figure 1. (a) As-received almond shells; **(b)** Processed almond shell flour (ASF).

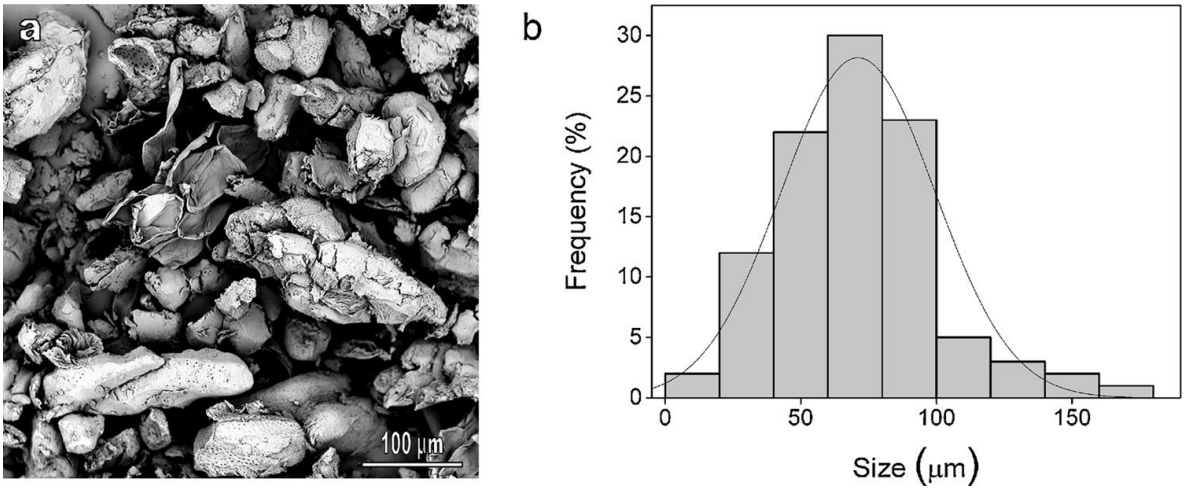

Figure 2. (a) Scanning electron microscope (SEM) image of almond shell flour (ASF). Image is taken with a magnification of 500× and a scale marker of 100 µm; **(b)** Histogram of ASF powder.

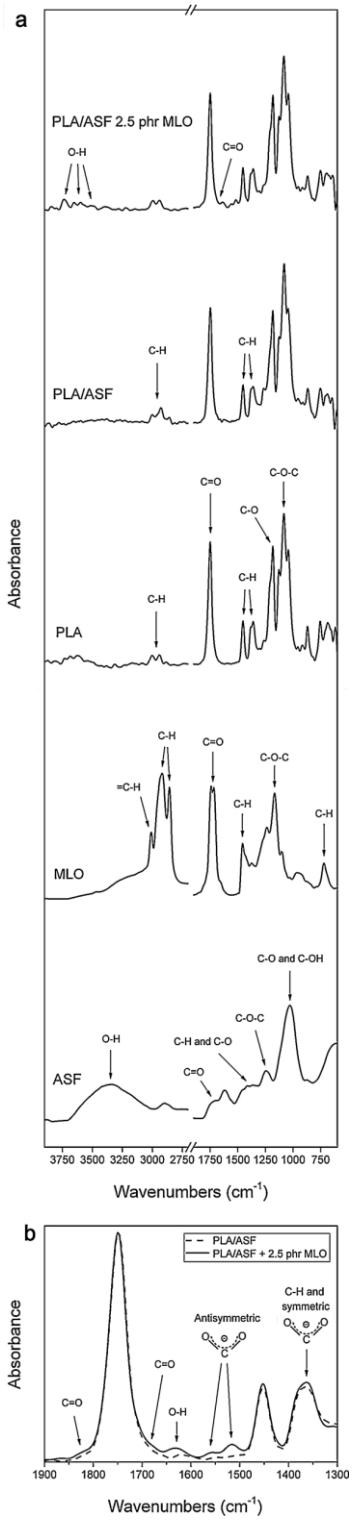

Figure 3. (a) Fourier transform infrared (FTIR) spectra, from bottom to top, of: Almond shell flour (ASF), maleinized linseed oil (MLO), polylactide (PLA), uncompatibilized PLA/ASF composite, and compatibilized PLA/ASF composite by 2.5 parts per hundred resin (phr) MLO. **(b)** Detail of the FTIR spectra for the uncompatibilized and compatibilized PLA/ASF composite. Arrows indicate the bands discussed in the text.

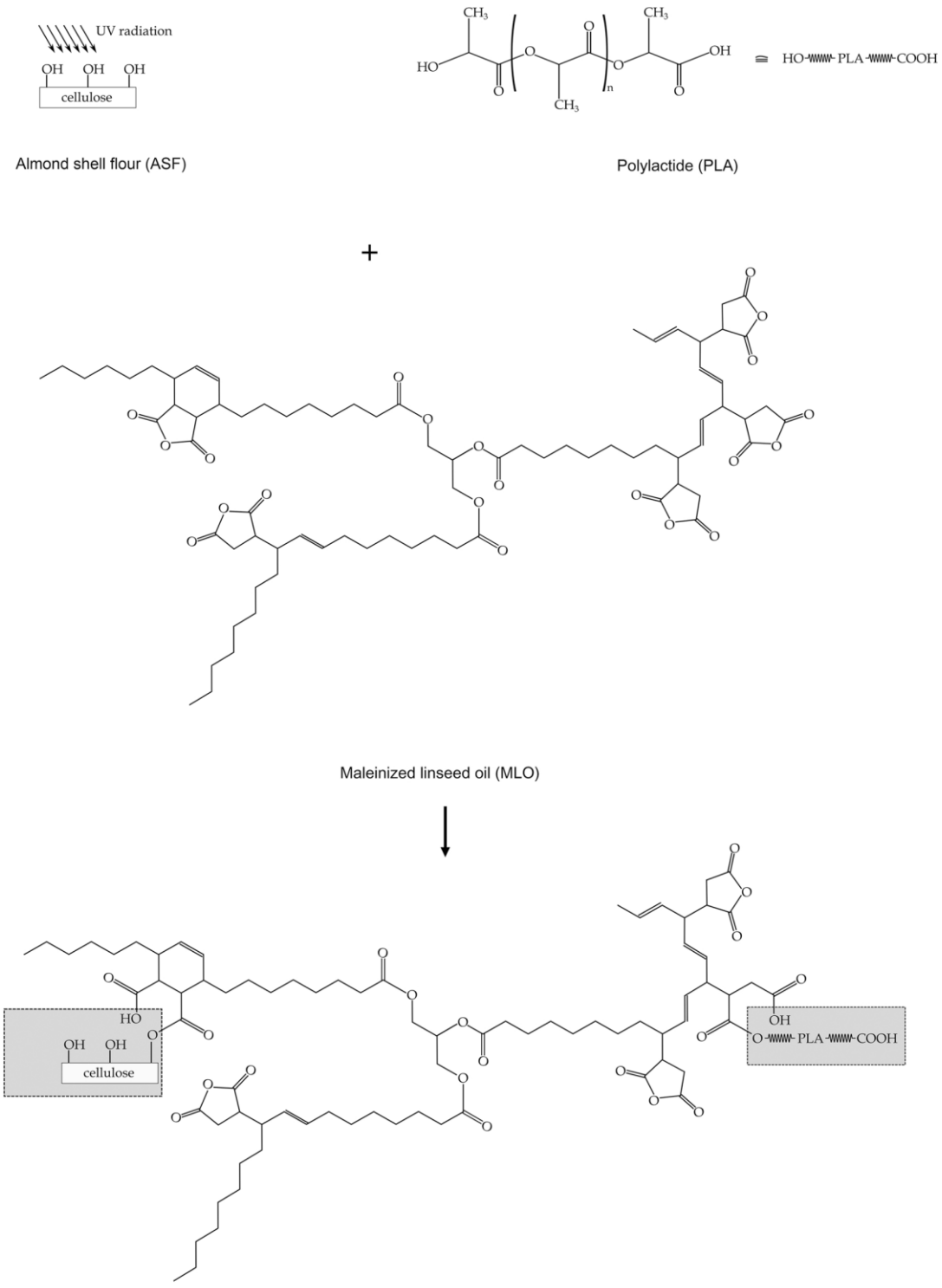

Figure 4. Schematic representation of the compatibilization between polylactide (PLA) with almond shell flour (ASF) by means of maleinized linseed oil (MLO).

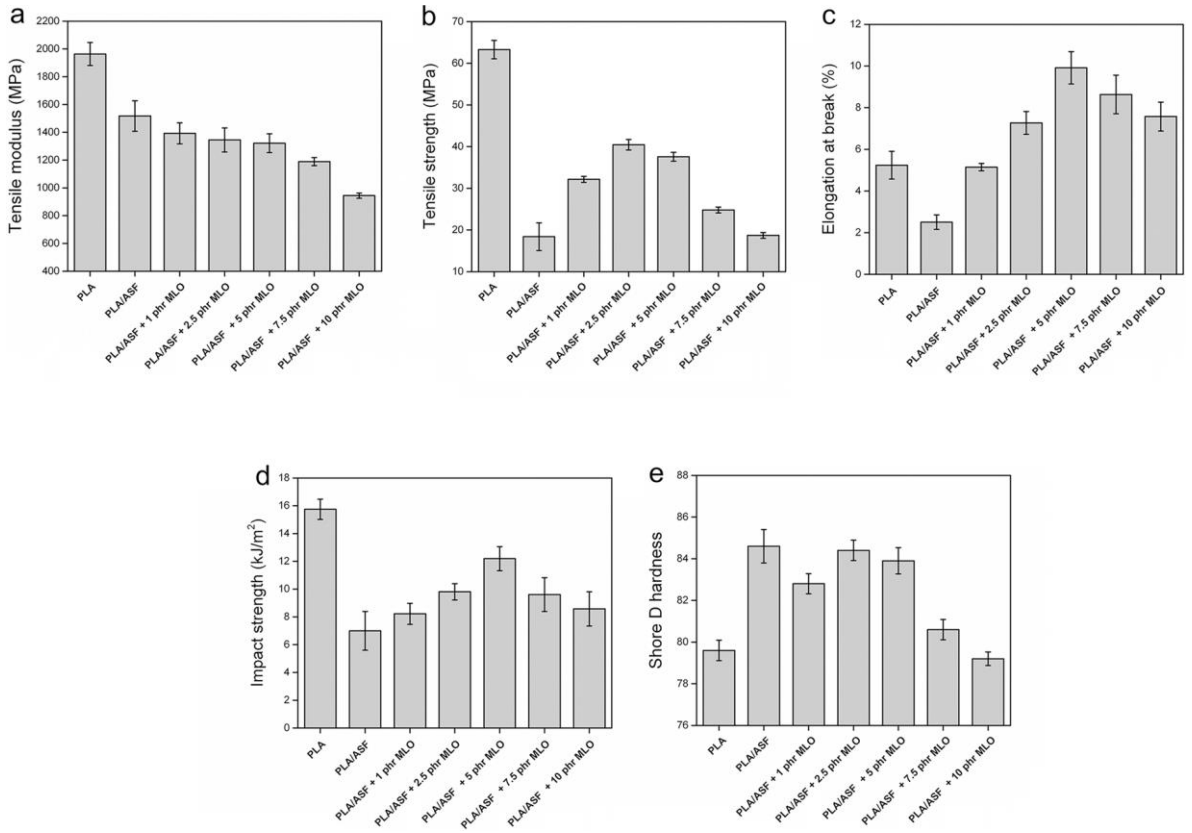

Figure 5. Mechanical properties of polylactide (PLA) and its green composites with almond shell flour (ASF) varying the content of maleinized linseed oil (MLO) in terms of: **(a)** Tensile modulus; **(b)** Tensile strength at yield; **(c)** Elongation at break; **(d)** Charpy impact strength; **(e)** Shore D hardness. MLO content is expressed as parts per hundred resin (phr).

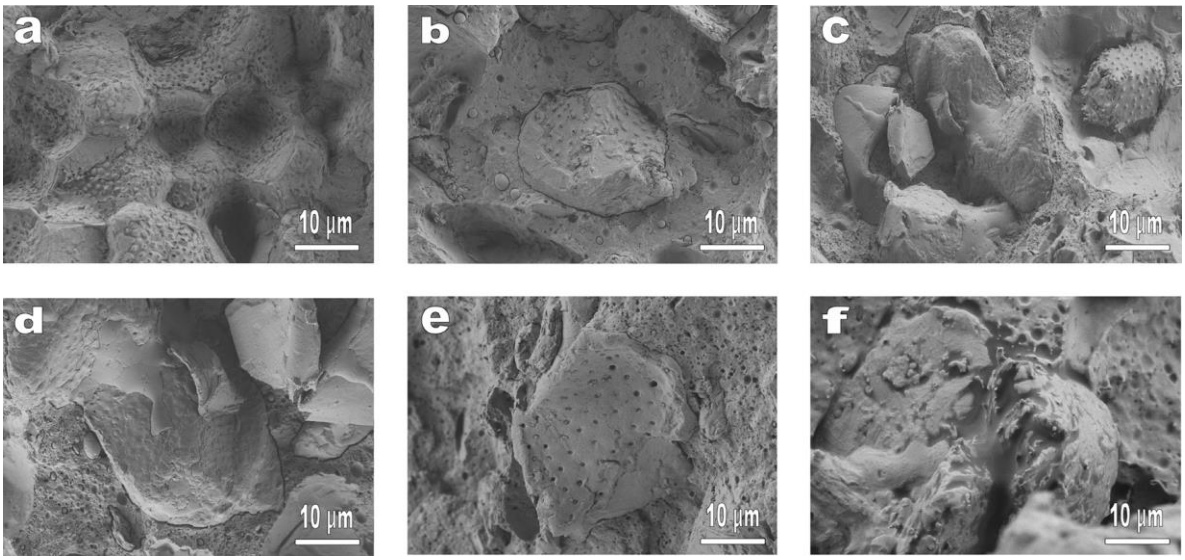

Figure 6. Scanning electron microscope (SEM) images of the fracture surfaces of: **(a)** Uncompatibilized polylactide (PLA)/almond shell flour (ASF) composite; **(b)** PLA/ASF composite compatibilized with 1 part per hundred resin (phr) maleinized linseed oil (MLO); **(c)** PLA/ASF composite compatibilized with 2.5 phr MLO; **(d)** PLA/ASF composite compatibilized with 5 phr MLO; **(e)** PLA/ASF composite compatibilized with 7.5 phr MLO; **(f)** PLA/ASF composite compatibilized with 10 phr MLO. Images are taken with a magnification of 1,500× and a scale marker of 10 µm.